Thermally activated processes and bias field effects on the electrical properties of BiFeO₃ thin films

Saulo Portes dos Reis[1], Fernando Brondani Minussi[2] and Eudes B. Araújo[3]

[1] *Federal Institute of Education, Science and Technology of São Paulo, 15503-110 Votuporanga, Brazil, spdreis@ifsp.edu.br*
[2] *Department of Physics and Chemistry, São Paulo State University, 15385-000 Ilha Solteira, Brazil, fbminussi@gmail.com*
[3] *Department of Physics and Chemistry, São Paulo State University, 15385-000 Ilha Solteira, Brazil, eudes.borges@unesp.br*

ABSTRACT

This work reports the temperature and electric field effects on the electrical properties of BiFeO₃ thin films. The increase in temperature promotes an increase in the dielectric permittivity of the studied film in the range of 100 Hz to 1 MHz, with a dielectric dispersion at the lower frequencies (~ 100 Hz), but no pronounced effects of the electric field on dielectric permittivity in the same frequency range were observed. The effects of temperature and electric on the electrical conductivity were also studied. Based on the obtained activation energy E = 0.40 eV, the conduction mechanism in the studied BiFeO₃ film was associated to the first ionization of oxygen vacancies.

1. INTRODUCTION

Known by a large ferroelectric polarization observed in thin films form [1], the BiFeO₃ (BFO) is a multiferroic material and as a promising material for the development of new spintronics devices based on the control of magnetization by an electric field [2]. On the other hand, due to a large leakage current at room temperature, the ferroelectric behavior of BiFeO₃ has proved to be a very difficult task from an experimental point of view, which further limits practical technological applications of BFO in the announced new multiferroic devices. In this scenario, grain boundaries in polycrystalline materials and impurities in single crystals are important points to consider as electrical measurements are very sensitive to these defects. Because these imperfections are more evident in polycrystalline samples than in BiFeO₃ single crystals, it is natural that higher leakage currents in polycrystalline thin films generally prevent the

application of high electric fields, making it difficult to measure a well-defined hysteresis loop. Thus, controlling defects in thin films of BFO, among other characteristics, has motivated continuous studies on the electrical properties of this multiferroic.

Electrical characterizations have been used to better understand the mechanisms behind the leakage current in BiFeO₃ thin films produced by different techniques and to understand the temperature and electrical field effects on these properties. The combination of complex impedance spectroscopy and electrical modulus spectroscopy has shown to be a powerful tool to study the dielectric relaxations of BiFeO₃ ceramics and thin films to infer about the influence of oxygen vacancies on the leakage current and its dielectric properties [3], the effects of Mn substitution on its electrical properties [4], the suppression of grain boundary relaxation in BFO films [5], and others. Usually, the non-Debye relaxation in multiferroic

thin films [6] or polycrystalline materials [7] is described in terms of the Cole-Cole model and subsequent generalizations to reveals the contributions of the grain, grain boundary and electrodes. However, a more realistic brick layer model can be alternatively used to describe the effects of inhomogeneous gains in electronic ceramics in terms of probability distributions [8], since the Cole-Cole model is not able to fit our data at lower frequencies. In this case, some effects that are not distinguished by the Cole-Cole model in the popular Nyquist diagram and other representations can be revealed using this statistical treatment [9]. These approaches indicate the importance of the electrical characterization as investigative tool to examine the dielectric relaxation and ac conductivity of BFO thin films for both academic and application point of view. In this article, we report the use of impedance formalism to discriminate thermally and electric field activated processes on the conductivity and permittivity of $BiFeO_3$ thin films prepared by chemical route.

2. FUNDAMENTALS AND BACKGROUND

2. 1. Impedance spectroscopy

Impedance spectroscopy is a technique widely used in the analysis of electrical properties of ceramics, ferroelectrics and mixed conductor [10]. The technique consists of placing the sample between two electrodes, forming a capacitor-like sample, then applying a variable voltage $V(t)$ and measuring the current obtained, $i(t)$, and its lag with respect to $V(t)$. In order to extract relevant physical parameters such as the electric conductivity and electric permittivity, it is essential to propose an equivalent circuit that is able to describe the experimental data [11]. To do this, we believe that a good mathematical understanding of the process and reasons for using impedance analysis is required.

Considering $V(t)$ the applied voltage and $i(t)$ the measured current, the complex impedance (Z^*) and complex admittance (Y^*) (the reciprocal of impedance) are defined as follow [12]:

$$Z^* = \frac{F\{V(t)\}}{F\{i(t)\}} \quad \text{and} \quad Y^* = \frac{F\{i(t)\}}{F\{V(t)\}} \tag{1}$$

where $F\{\ \}$ denotes the Fourier transform operator. From equation (1) we obtain that the impedance of a resistor with a resistance R and a capacitor of capacitance C are respectively given by $Z_R^* = R$ and $Z_C^* = (j\omega C)^{-1}$, where ω is the angular frequency of the applied signal and $j^2 = -1$. The great advantage of defining impedance through Fourier transforms lies in the operator linearity, which imposes that the impedance association has the same rules as the resistor associations.

Non-localized diffusion processes can be described by a circuit constructed by a parallel association between a resistor and a capacitor [13], so the impedance and admittance of these processes are respectively given by:

$$Z^* = \frac{R}{1 + j\omega RC} \quad \text{and} \quad Y^* = \frac{1}{R} + j\omega C \tag{2}$$

where the RC product is named as relaxation time represented by τ. Since S and l are the sample geometrical parameters (area and thickness, respectively), the above equations indicate that the electrical conductivity and permittivity are constant, i.e., do not depend on ω. The representation given above is not accurate when the dynamic processes acting on the system in question have very close distribution times, which causes a dispersion in both conductivity and permittivity. In this case we should consider a distribution of relaxation times [13].

2. 2. Relaxation times distribution: discrete case

It is commonly recognized that the impedance response of a particular material can be simulated by more than one equivalent electrical circuit to describe its bulk and grain boundaries contributions, but researchers tend to use the most appropriate circuit to explain their results in a realistic scenario without inconsistences. To represent different conductivity processes in a given material, the equivalent circuit illustrated in Figure 1 can be used.

We note that each RC component of the circuit has a characteristic relaxation time. Considering that $\tau_k = R_k C_k$, it follows:

$$Z^* = \sum_{k=1}^{n} \frac{R_K}{1 + j\omega\tau_k} \quad \text{and} \quad Y^* = \left(\sum_{k=1}^{n} \frac{1}{\frac{1}{R_k} + j\omega C_k} \right)^{-1}. \tag{3}$$

26

Nanomater. Sci. Eng., Vol. 2, No. 1, pp. 25-34 (2020)

RESEARCH ARTICLE
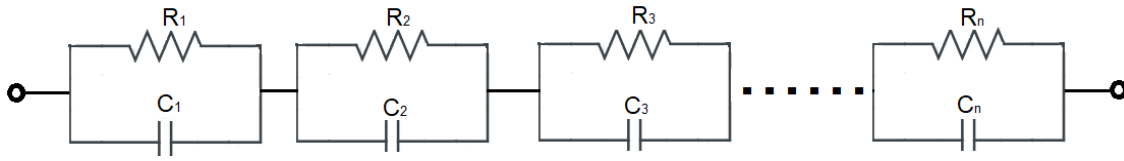
Figure 1. Representation of *n* parallel RC circuits in associated in series to represent different relaxation times.

The admittance equation allows us to obtain the profile of the dispersions of the real components of conductivity and permittivity, respectively:

$$\sigma'(\omega) = \frac{\Sigma\left(\dfrac{\sigma_k}{\sigma_k^2 + \omega^2\epsilon_0^2\epsilon_k^2}\right)}{\left[\Sigma\left(\dfrac{\sigma_k}{\sigma_k^2 + \omega^2\epsilon_0^2\epsilon_k^2}\right)\right]^2 + \omega^2\left[\Sigma\left(\dfrac{\epsilon_0\epsilon_k}{\sigma_k^2 + \omega^2\epsilon_0^2\epsilon_k^2}\right)\right]^2} \tag{4}$$

$$\epsilon'(\omega) = \frac{\Sigma\left(\dfrac{\epsilon_k}{\sigma_k^2 + \omega^2\epsilon_0^2\epsilon_k^2}\right)}{\left[\Sigma\left(\dfrac{\sigma_k}{\sigma_k^2 + \omega^2\epsilon_0^2\epsilon_k^2}\right)\right]^2 + \omega^2\left[\Sigma\left(\dfrac{\epsilon_0\epsilon_k}{\sigma_k^2 + \omega^2\epsilon_0^2\epsilon_k^2}\right)\right]^2} \ . \tag{5}$$

On the limit for low frequencies:

$$\lim_{\omega\to 0}\sigma(\omega) = \sigma_{dc} = \frac{1}{\dfrac{1}{\sigma_1} + \dfrac{1}{\sigma_2} + \cdots + \dfrac{1}{\sigma_n}} \quad \text{and} \quad \lim_{\omega\to 0}\epsilon(\omega) = \frac{\dfrac{\epsilon_1}{\sigma_1^2} + \dfrac{\epsilon_2}{\sigma_2^2} + \cdots + \dfrac{\epsilon_n}{\sigma_n^2}}{\left(\dfrac{1}{\sigma_1} + \dfrac{1}{\sigma_2} + \cdots + \dfrac{1}{\sigma_n}\right)^2} \ , \tag{6}$$

and, for high frequencies:

$$\lim_{\omega\to+\infty}\sigma(\omega) = \frac{\dfrac{\sigma_1}{\epsilon_1^2} + \dfrac{\sigma_2}{\epsilon_2^2} + \cdots + \dfrac{\sigma_n}{\epsilon_n^2}}{\left(\dfrac{1}{\epsilon_1} + \dfrac{1}{\epsilon_2} + \cdots + \dfrac{1}{\epsilon_n}\right)^2}, \quad \text{and} \quad \lim_{\omega\to+\infty}\epsilon(\omega) = \epsilon_r = \frac{1}{\dfrac{1}{\epsilon_1} + \dfrac{1}{\epsilon_2} + \cdots + \dfrac{1}{\epsilon_n}} \ . \tag{7}$$

Equations (6) and (7) indicate that low frequency electrical conductivity (σ_{dc}) is dominated by the lowest conductivity element, but at high frequencies the conductivity shows an intrinsic permittivity dependence. Similarly, the electric permittivity is influenced by conductivity in low frequencies and is dominated by the element of lowest permittivity at high frequencies.
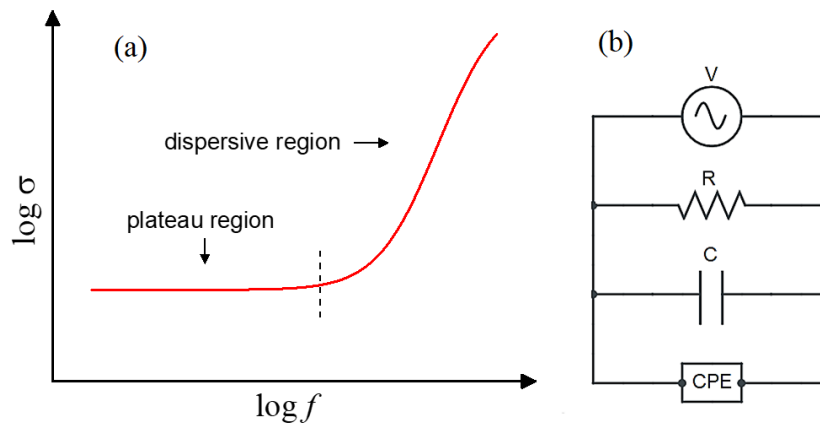
Figure 2. (a) Typical log–log real conductivity (σ) versus frequency relationship at a given temperature for conductive materials. (b) The used model to describe the conductivity in (a). times.

2. 3. Relaxation times distribution: continuous case

Switching to the continuous case requires a density function that represents the distribution of resistor and capacitance values. In this case, the impedance equation is given by:

$$Z^* = \int_0^\infty \frac{G(\tau)d\tau}{1+j\omega\tau},\qquad(8)$$

where $G(\tau)$ represents the total resistance over a relaxation time interval $d\tau$. The solution of this integral can be difficult to obtain even for simple functions (as seen in [14]). However, in addition to the mentioned elements of the circuit, the inclusion of constant phase elements (CPE's), such as $Z_{CPE}^* = (jA\omega)^{-n}$, representing the departures from Debye-like ideality of each component, describes the distribution of relaxation times with the distribution parameter A, as proposed by Cole-Cole [15]. Since an ideal Debye-like response was never obtained, the impedance response cannot be treated in terms of simple parallel RC elements. Thus, the inclusion of the CPE element is comprehensive to fit the experimental frequency dependence of real conductivity, as shown in Figure 2(a). The CPE element describes the so-called Jonsher's law [16]. In summary, the RC-CPE circuit shown in Figure 2(b) is used to describe the grain boundaries impedance in polycrystals materials.

Considering the model described by the electrical circuit shown in Figure 2(b), the real components of the electric conductivity and the electric permittivity are given by:

$$\sigma'(\omega) = \sigma_{dc} + A'\,\omega^n \cos\left(\frac{n\pi}{2}\right)\qquad(9)$$

$$\epsilon'(\omega) = \epsilon_r + \frac{A'}{\epsilon_0\omega^{1-n}}\,sin\left(\frac{n\pi}{2}\right),\qquad(10)$$

where $A' = (Al)/S$, $\sigma_{dc} = l/(RS)$ and $\epsilon_r = (Cl)/(\epsilon_0 S)$. It should be noted that the conductivity equation is in the form $\sigma(\omega) = \sigma_{dc} + B\omega^n$, as attributed by Jonscher [16]. These two equations above are in agreement with what was discussed in the discrete case, as the electric conductivity converges at low frequencies, while dielectric permittivity converges at high frequencies. Moreover, the term A' contained in the CPE is responsible for accounting the dispersion of both the resistance (conductivity) and the capacitance (permittivity) of a sample, so we can infer that the CPE simplifies the expressions containing the quadratic terms of electric permittivity and electric conductivity.

2.4. Thermally activated conductivity

Many ceramic materials conduct electricity through ion migration [17]. This ionic conductivity involves the migration of charge carriers (ions) over long distances and, being this process thermally activated, then its temperature dependence is typically described by an Arrhenius type expression such as [18]:

$$\sigma_{dc} = \sigma_0 exp\left(\frac{-E_a}{kT}\right),\qquad(11)$$

28

Nanomater. Sci. Eng., Vol. 2, No. 1, pp. 25-34 (2020)

RESEARCH ARTICLE
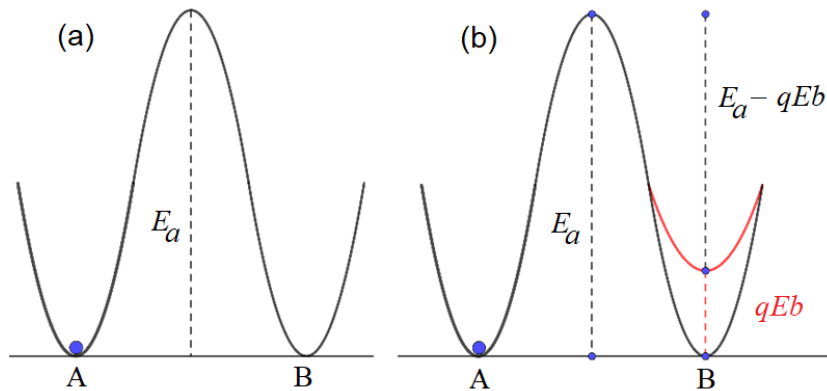
Figure 3. Energy levels before (a) and after (b) the application of a bias electric field E. In this figure, E_a is the activation energy, q the charge carrier and b the jump distance.

where σ_0 is a pre-exponential parameter, k is the Boltzmann constant and E_a the activation energy of a given ionic conduction process. The activation energy for ionic conduction, as illustrated in Figure 3(a), consists of the energy barrier of the lowest resistance path [9]. In order to a charge carrier to migrate, a minimum energy corresponding to this activation energy must be provided. In the absence of an energy difference between the positions given by A and B in Figure 3(a), there is no net movement of the charge carriers in a given direction, *i.e.*, the probability of jump from A to B is equal to the probability of jump from B to A. However, once an electric potential difference is applied, as shown in Figure 3(b), an electric field arises and causes an imbalance between the energies at positions A and B.

Considering the presence of a bias electric field *E*, the energy difference (ΔU) between positions A and B can be given by:

$$\Delta U = qEb, \tag{12}$$

where *q* is the carrier charge and *b* is the distance between A and B, which are the lowest energies of the respective potential wells (or the equilibrium points). Taking this energy configuration, it is observed that the potential barrier for a jump from A to B is different from that of the jump from B to A, resulting in an imbalance of the jump probability. In other words, the bias electric field disturbs the initially random thermal motion, increasing the probability of transition in the direction of field application to a cation and in the reverse direction to an anion. So, in the presence of a bias electric

field, there is a decreasing of the potential barrier for a jump from B to A. Calling this decreasing as E_{eff} barrier, it follows that for a thermally activated process:

$$\sigma_{dc} = \sigma_0 exp\left(\frac{-E_{eff}}{kT}\right). \tag{13}$$

Observing that $E_{eff} = E_a - \Delta U = E_a - qEb$, it follows that:

$$\sigma_{dc} = \sigma_0 exp\left(\frac{-E_a + qEb}{kT}\right). \tag{14}$$

From Equations (13) and (14) it is observed that $ln(\sigma_{dc})$ decreases with the reciprocal temperature and increases with the bias electric field, resulting essentially in the same response, which is the conductivity increasing of an ionic process. However, it should be emphasized that for a rise in temperature, this behavior is a consequence of the higher energy available to the system to overcome the energy barrier of an ionic conduction process, which is, in a first approximation, constant with the temperature. In turn, under an applied electric field the energy barrier will change resulting in a smaller "effective" activation energy. According to the Equation (14), it should be noted that the ionic mobility is not null for a situation where there is not an applied electric field, but, for a hypothetical absolute zero condition, the migration would not be possible. In other words, we can interpret that the role of temperature is to provide mobility to charge carriers, while the electric field provides a preferential direction of migration. For a such temperature, Equation (14) can be rewritten to describe the electric field dependence such as:

29

$$ln(\sigma_{dc}) = a_1 + a_2 E, \qquad (15)$$

where $a_1 = ln(\sigma_0) - \dfrac{E_a}{kT}$ and $a_2 = \dfrac{qb}{kT}$.

3. EXPERIMENTAL PROCEDURE

In the present work, BiFeO$_3$ thin films were prepared by a chemical solution route dissolving appropriate amounts of bismuth nitrate pentahydrate Bi(NO$_3$)$_3$.5H$_2$O (Sigma-Aldrich, 99.9%) and iron nitrate nonahydrate Fe(NO$_3$)$_3$.9H$_2$O (Sigma-Aldrich, 99.9%) into a solution composed by 1 mL of 2-methoxyethanol (Sigma-Aldrich, 99.9%) and 5 mL of glacial acetic acid (Sigma-Aldrich, 99.9%), at 50°C under magnetic stirring for 10 min. After complete homogenization, the temperature of the solution was raised to 80°C and kept under stirring for 30 min. Finally, after cooling to room temperature, 3 mL of glacial acetic acid was added to obtain a 0.16 M solution after filtering it using a microfiber filter paper.

Films of the precursor solution were deposited (4 depositions) on Pt/TiO$_2$/SiO$_2$/Si(100) substrates by spin-coating at 5000 rpm for 30 seconds. After the solution deposition, the films were placed directly on a hot-plate at ~ 200°C for 5 min to remove water, and then annealed in an electric furnace at 300°C for 30 min to remove organics. By following the same procedure, additional layers were deposited on the previously annealed film to increase its thickness. Next, the films were crystallized in air at 600°C for 40 min and finally post annealed at 600°C for 5 hours in O$_2$ atmosphere. The thickness of the final film is found to be ~ 500 nm. For electrical measurements,

circular Au top electrodes of 0.30 mm diameter were sputtered on the film surfaces by using a shadow mask. An Agilent 4284A LCR meter was used to measure the complex impedance in the frequency, temperature and bias electrical field ranges of 100 - 10^6 Hz, 335 - 420 K (with no bias field) and 0 - 22 kV.cm^{-1} (room temperature), respectively.

4. RESULTS AND DISCUSSION

Figure 4 shows the variation of real dielectric permittivity (ε') of the studied BiFeO$_3$ thin film in the frequency range of 100 Hz to 1 MHz, at different temperatures (a) and bias electric field (b). In Figure 4(a), the value of permittivity falls with frequency increasing, but at the lower frequency it reaches higher values. In other words, at frequencies lower than 10 kHz a pronounced dielectric dispersion is observed while at higher frequencies the permittivity tends to a frequency independent value ($\varepsilon_\infty \sim 26$). On the other hand, at higher temperatures the dielectric permittivity increases, such that the temperature effects are less pronounced at higher frequencies than at low frequencies, where a dielectric dispersion is observed, as shown in Figure 4(a). In contrast to the effects of temperature, similar dielectric dispersions on dielectric permittivity were not observed by applying different external dc electric field, as shown in Figure 4 (b). The dielectric permittivity behavior in this figure was essentially the same for different electric field in the studied frequency range and, under the electric field effects, the frequency independent permittivity tends to $\varepsilon_\infty \sim 36$.
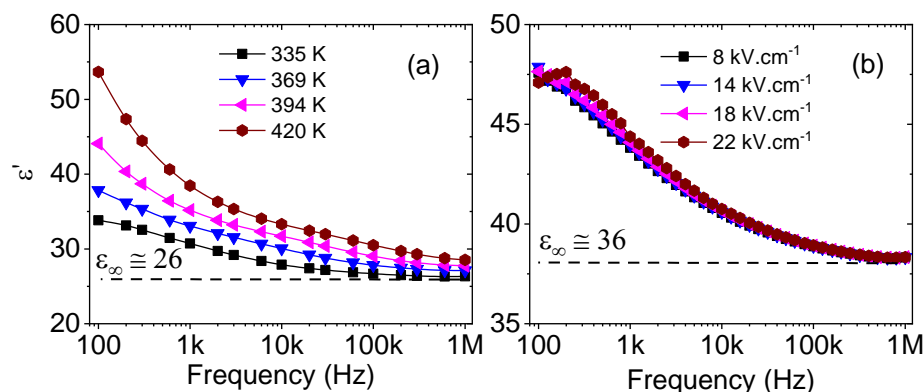
Figure 4. Frequency dependence of the real permittivity for BiFeO$_3$ thin film obtained from impedance measurements at (a) different temperatures and (b) different bias electric field.

Nanomater. Sci. Eng., Vol. 2, No. 1, pp. 25-34 (2020)

RESEARCH ARTICLE

The presence of different polarizations, such as ionic, dipolar and space-charge, may be responsible for higher permittivity values at lower frequencies, but at higher frequencies some of them do not follow the alternating field, so their contribution to permittivity decrease or disappear resulting in lower permittivity values. It is well known that electronic polarization predominates in the high-frequency region [19]. The dielectric dispersion observed at low frequencies can be explained by the greater interference of grain effects over grain boundary effects, which is attributed to Maxwell–Wagner type of interfacial polarization in accordance with Koop's phenomenological theory [20]. The presence of space charge polarization at the grain boundaries generates a potential barrier responsible for the observed high values of the real part of permittivity. The decrease of the real part of permittivity at higher frequencies can be understood if we consider that low resistive grains are separated by grain boundaries with lower conductivity in dielectric, as shown in Equation (7). Thus, regarding the temperature effects, it is expected that dielectric permittivity increases with increasing temperature, and this increase is higher in the dielectric dispersion at lower frequencies, as

demonstrates Equation (6) and as shown in Figure 4(a). This dielectric dispersion at low temperatures agree with those observed in typical ferroelectrics [21], as well as for $BiFeO_3$ thin films prepared by chemical solution deposition method [22]. As a result of the applied electric field, a localized accumulation of charges occurs leading to the interfacial polarization [23]. In Figure 4(b), no pronounced effects of bias electric field on dielectric permittivity suggest that the DC electric field causes a saturation of spatial charge. The difference between independent permittivity values is attributed to difference between relaxation times in the two process. As mentioned before, we can define $\tau = RC$ as the relaxation time, which leads to:

$$\tau = RC = \epsilon_0 \epsilon_r \frac{1}{\sigma_{DC}} . \tag{16}$$

Therefore, a change in the relaxation time causes a change in the relative permittivity. This difference probably due to a higher concentration of special loads caused by applying a DC field.

Figure 5(a) shows the frequency dependence of the conductivity while Figure 5(b) shows Nyquist plots of Z′ versus Z″ of the studied $BiFeO_3$ thin film at different temperatures (top) and different bias
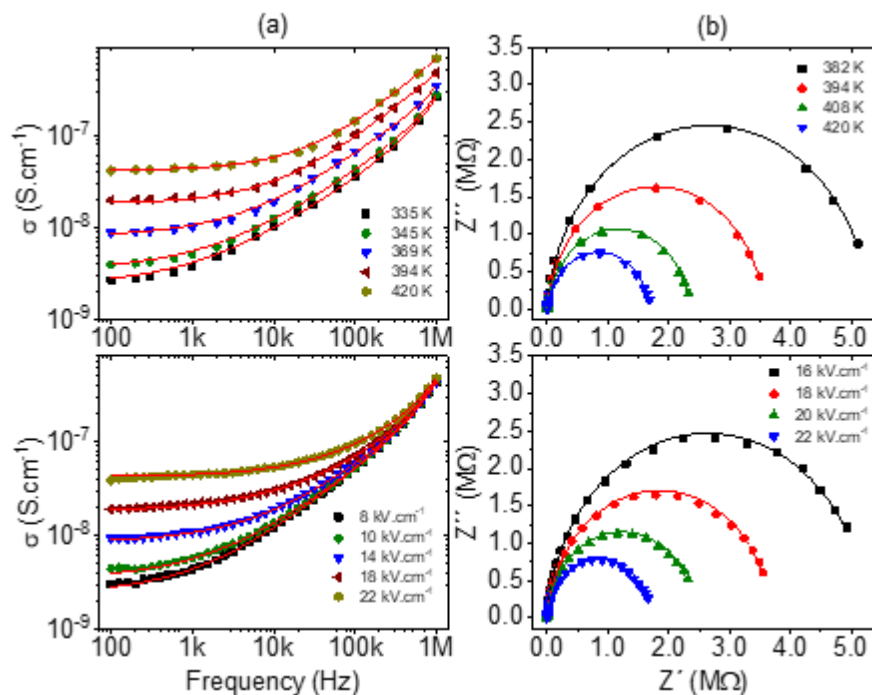
Figure 5. (a) Frequency dependence of the conductivity and (b) Nyquist plots of Z′ versus Z″ for $BiFeO_3$ thin film at different temperatures (top) and different bias electric field (bottom). Symbols are experimental data and lines are theoretical fits (R-C-CPE model).

31

electric field (bottom). Lines in Figure 5(a) top are theoretical fits from Jonscher model described in Equation (9), which are in good agreement with experimental data. It was observed in Figure 5(a) that the temperature and electric field effects on electrical conductivity at low frequencies (σ_{dc}) were essentially the same. In other words, the σ_{dc} increases when both temperature and electric field increases, as predicted by Equations (11) and (14). However, the conductivity shows a temperature dependence at higher frequencies while the high-frequency conductivity is electric field independent. Nyquist plots in Figure 5(b) shows the same temperature and electric field effects in another perspective. Since the diameter of the semicircles in the impedance diagram represents the resistance, the decrease observed in the semicircles with increasing temperature and electric field corroborates the increase in conductivity observed in Figure 5(a).

From theoretical fits to the experimental data shown in Figure 5(a) at the top, the obtained dc conductivities were plotted in Figure 6(a) as a function of the temperature. Based on linear fit in this figure, the obtained activation energy was 0.40

eV. This activation energies are in good agreement with those values reported for BFO thin films prepared by rf sputtering [24]. In general, activation energies around 0.28 eV are associated to the first ionization of oxygen vacancies in perovskite structure of Bi-doped $SrTiO_3$ ceramics [25]. Thus, the obtained activation energy in the present work suggests that the conduction mechanism in studied $BiFeO_3$ can be associated to the first ionization of oxygen vacancies. Considering the temperature and electric field that led to the same dc electric conductivity in the sample, as example the data obtained at 334.8K had the same electric conductivity as the obtained with a field of 8 kV.cm^{-1} and so on, dc conductivity of the $BiFeO_3$ thin film was plotted in Figure 6(b) as a function of electric field, where a slope of 0.20 was obtained. On the other hand, the linear behavior in Figure 6(c) shows the temperature as a function of the electric field. Since the slope in this curve is 6.12, we can conclude that an increase of the 1 kV.cm^{-1} should result in the same variation in the dc conductivity of an increase of 6.12 K in temperature.
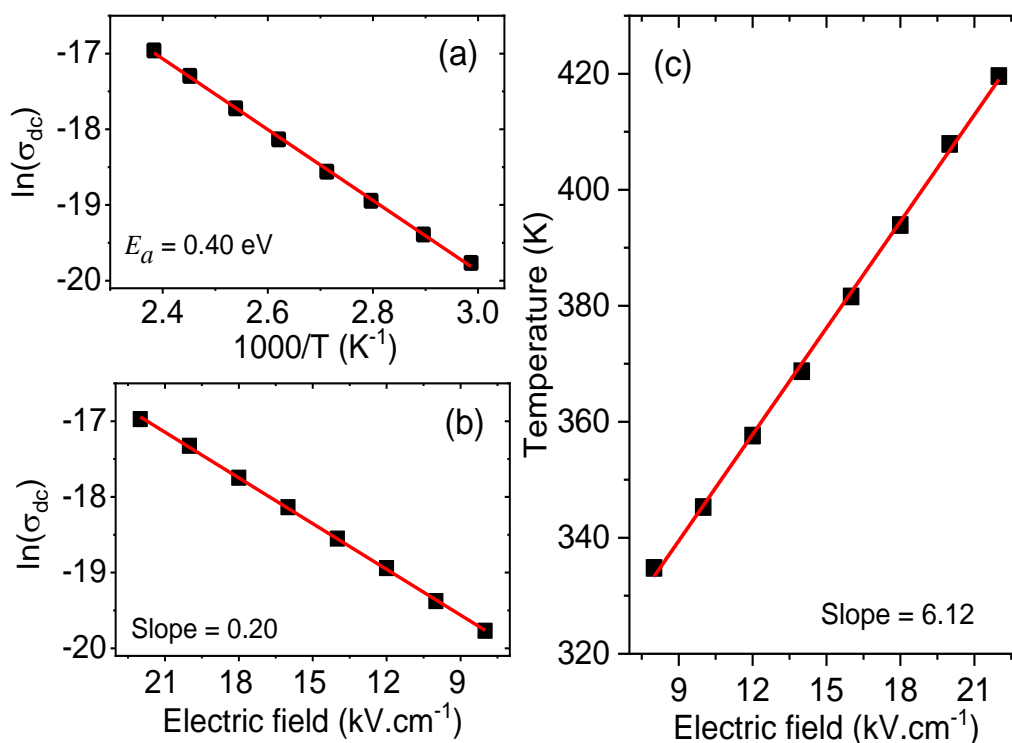
Figure 6. DC conductivity as a function of (a) reciprocal temperature and (b) electric field for $BiFeO_3$ thin film. (c) Electric field dependence of temperature. Red lines are linear fits.

Nanomater. Sci. Eng., Vol. 2, No. 1, pp. 25-34 (2020)

RESEARCH ARTICLE
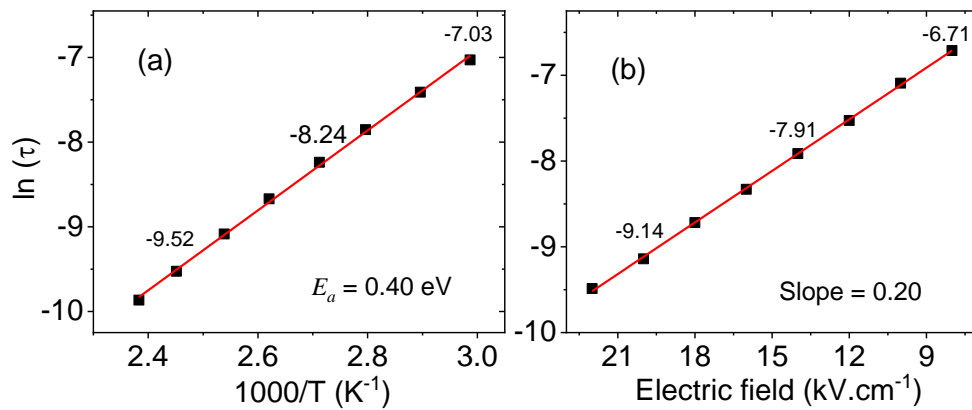
Figure 7. Relaxation time as a function of (a) reciprocal temperature and (b) electric field for BiFeO₃ thin film.

Finally, relaxation times as a function of temperature and bias electric field were plotted in Figures 7(a) and 7(b), respectively. Although the activation energy of 0.40 eV and the slope of 0.2 in these figures were the same values as obtained in Figures 6(a) and 6(b), point values presented in Figures 7(a) and 7(b) indicate that a difference in the value of the relaxation times exists a difference in the value of the relaxation times, although the dc conductivity is the same. This fact was first identified in the Figure 5(a), where the temperature and electric field effects on conductivity are different at higher frequencies. Equation (7) shows that the conductivity is affected by permittivity at high frequencies, indicating that the difference between relaxation times occurs because the electric field and the temperature change the capacitance of the sample in a different manner.

5. CONCLUSIONS

The temperature and electric field effects on the electrical properties of BiFeO₃ thin film were studied. The dielectric permittivity of the studied BiFeO₃ film increases by increasing the temperature and this increasing is higher in the dielectric dispersion at lower frequencies, while no pronounced effects of bias electric field on dielectric permittivity were observed. The conductivity at low frequencies (σ_{dc}) increases when both temperature and electric field increases, but the conductivity shows a temperature dependence at higher frequencies while the high-frequency conductivity is electric field independent. The obtained activation energies around 0.40 eV indicate that the conduction mechanism in the

studied BiFeO₃ film is associated to the first ionization of oxygen vacancies.

REFERENCES

[1] J. Wang, J. B. Neaton, H. Zheng, V. Nagarajan, S. B. Ogale, B. Liu, D. Viehland, V. Vaithyanathan, D. G. Schlom, U. V. Waghmare, N. A. Spaldin, K. M. Rabe, M. Wuttig, and R. Ramesh, Epitaxial BiFeO₃ multiferroic thin film heterostructures, *Science.* **299**, 1719 (2003).

[2] M. Bibes, and A. Barthelemy, Multiferroics: towards a magnetoelectric memory, *Nat. Mater.* **7** (6), 425 (2008).

[3] Y.W. Li, Z.G. Hu, F.Y. Yue, P.X. Yang, Y.N. Qian, W.J. Cheng, X.M. Ma, J.H. Chu. Oxygen-vacancy-related dielectric relaxation in BiFeO₃ films grown by pulsed laser deposition. *J. Phys. D: Appl. Phys.* 2008; 41: 215403.

[4] D.K. Pradhan, R.N.P. Choudhary, C. Rinaldi, R.S. Katiyar. Effect of Mn substitution on electrical and magnetic properties of Bi₀.₉La₀.₁FeO₃. *J. Appl. Phys.* 2009; 106: 024102.

[5] S. Mukherjee, A. Srivastava, R. Gupta, A. Garg. Suppression of grain boundary relaxation in Zr-doped BiFeO₃ thin films. *J. Appl. Phys.* 2014; 115: 204102.

[6] R. Schmidt, W. Eerenstein, T. Winiecki, F.D. Morrison, P.A. Midgley: Impedance spectroscopy of epitaxial multiferroic thin films. *Phys Rev B.* 2007; 75: 245111.

[7] N. Ortega, A. Kumar, P. Bhattacharya, S.B. Majumder, R.S. Katiyar: Impedance spectroscopy of

multiferroic $PbZr_xTi_{1-x}O_3/CoFe_2O_4$. *Phys Rev B.* 2008; 77: 014111.

[8] M. Vollmann, R. Hagenbeck, R. Waser. Grain-boundary defect chemistry of acceptor-doped titanates: Inversion layer and low-field conduction. *J. Am. Ceram. Soc.* 1997; 80: 2301-2314.

[9] S. Song, F. Placido. The influence of phase probability distributions on impedance spectroscopy. *J. Stat. Mech.: Theory Exp.* 2004; P10018.

[10] E. J. Abram, D. C. Sinclair and A. R. West, *J. Electroceram.*, **10**, 165-177 (2003).

[11] A. R. West, D. C. Sinclair and N. Hirose, *J. Electroceram.*, **1**(1), 61-75 (1997).

[12] E. Barsoukov, J. R. Macdonald, Impedance spectroscopy: theory, experiment and applications, 3rd ed. John Wiley & Sons, New Jersey (2018)

[13] W. Cao and R. Gerhardt, *Solid State Ionics*, **42**, 213-221 (1990).

[14] S. Song and F. Placido, *J. Stat. Mech.*, P10018 (2004).

[15] K. S. Cole and R. H. Cole, *J. Chem. Phis.*,**9**, 341 (1941).

[16] A. K. Jonscher, Dielectric relaxation in solids, Chelsea Dielectric Press, London (1983)

[17] Y-T. Chiang, P. B. Birnie and W. D. Kingery, Physical ceramics: principles for ceramic science and engineering, John Wiley & Sons, New Jersey (1996).

[18] L. L. Hench and J. K. West, Principles of electronic ceramics, John Wiley & Sons, New Jersey (1990).

[19] S. Hajra, S. Sahoo, R. Das, R.N.P. Choudhary, *J. Alloy. Comp.* **750**, 507-514 (2018).

[20] C. G. Koops *Phys. Rev.* **83**, 121 (1951).

[21] J. F. Araújo, J. Mendes Filho, F. E. A. Melo, F. V. Letelier and A. S. Chaves. *Phys. Rev. B* **57**, 783-788 (1998).

[22] S. Mukherjee, A. Srivastava, R. Gupta and A. Garg, *J. Appl. Phys.* 115, 204102 (2014).

[23] H. Rahmouni, M. Smari, B. Cherif, E. Dhahri and K. Khirouni, *Dalton Trans.* **44**, 10457-10466 (2015).

[24] J. Wu, and J. Wang, Ferroelectric and impedance behavior of La-and Ti-codoped $BiFeO_3$ thin films, *J Am Ceram Soc.* **93** (9), 2795 (2010).

[25] C. Ang, Z. Yu, and L. E. Cross, ''Oxygen-Vacancy-Related Low-Frequency Dielectric Relaxation and Electrical Conduction in Bi: $SrTiO_3$,'' *Phys. Rev. B,* **62**, 228 (2000).

34